Robust and perfectible constraints on human-induced Arctic amplification

Hervé Douville[1]

[1] *Centre National de Recherches Météorologiques, Université de Toulouse, Météo-France, CNRS, 42 Avenue Gaspard Coriolis, 31057 Toulouse, France*

Corresponding author: Hervé Douville (herve.douville@meteo.fr)

Content: Supplementary Fig. S1 to Fig. S18 further supporting our key findings.

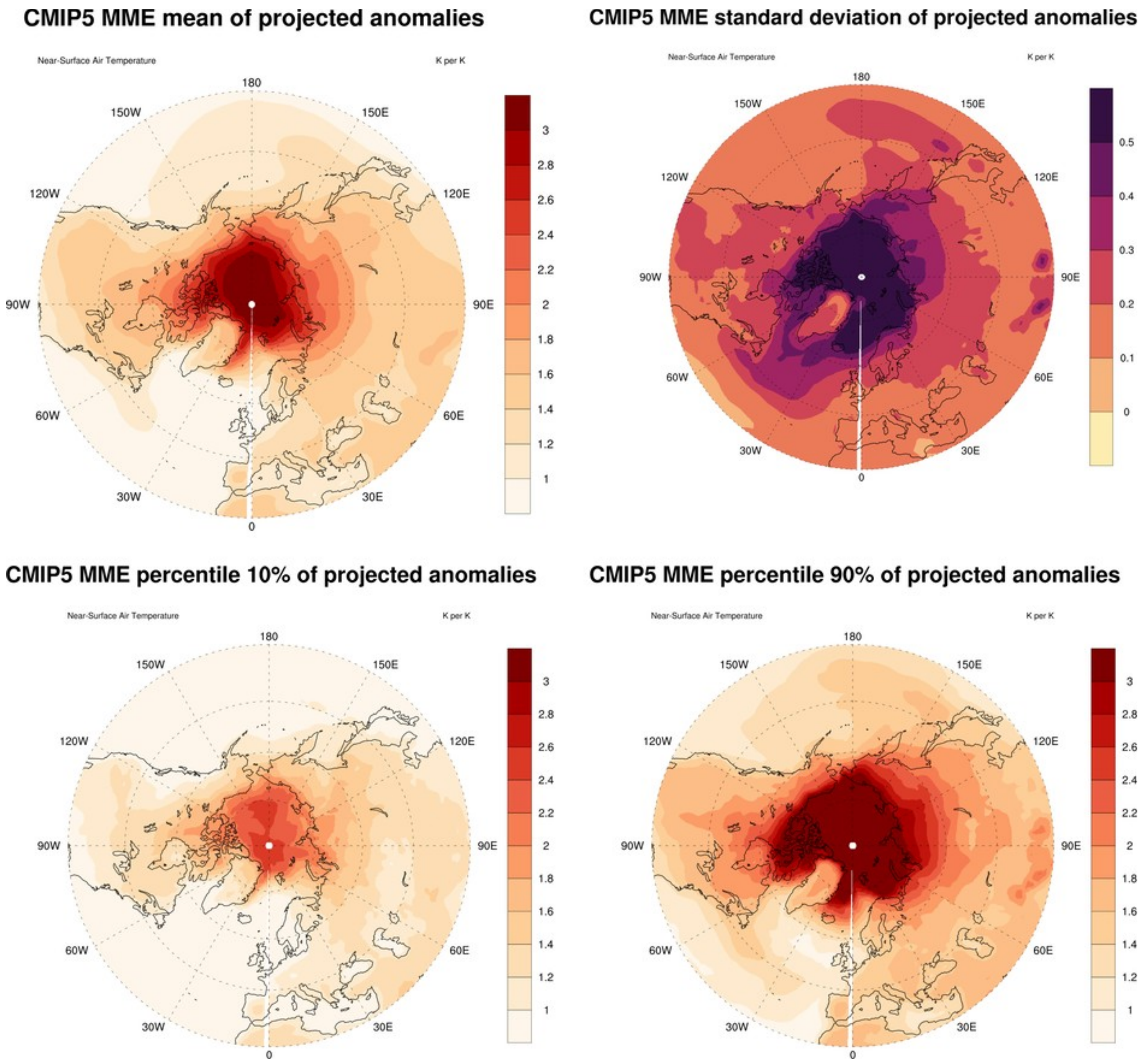

Fig. S1: Same as Fig. 1 but for the CMIP5 (RCP8.5) rather than CMIP6 high-emission scenario (K per 1K of global warming).

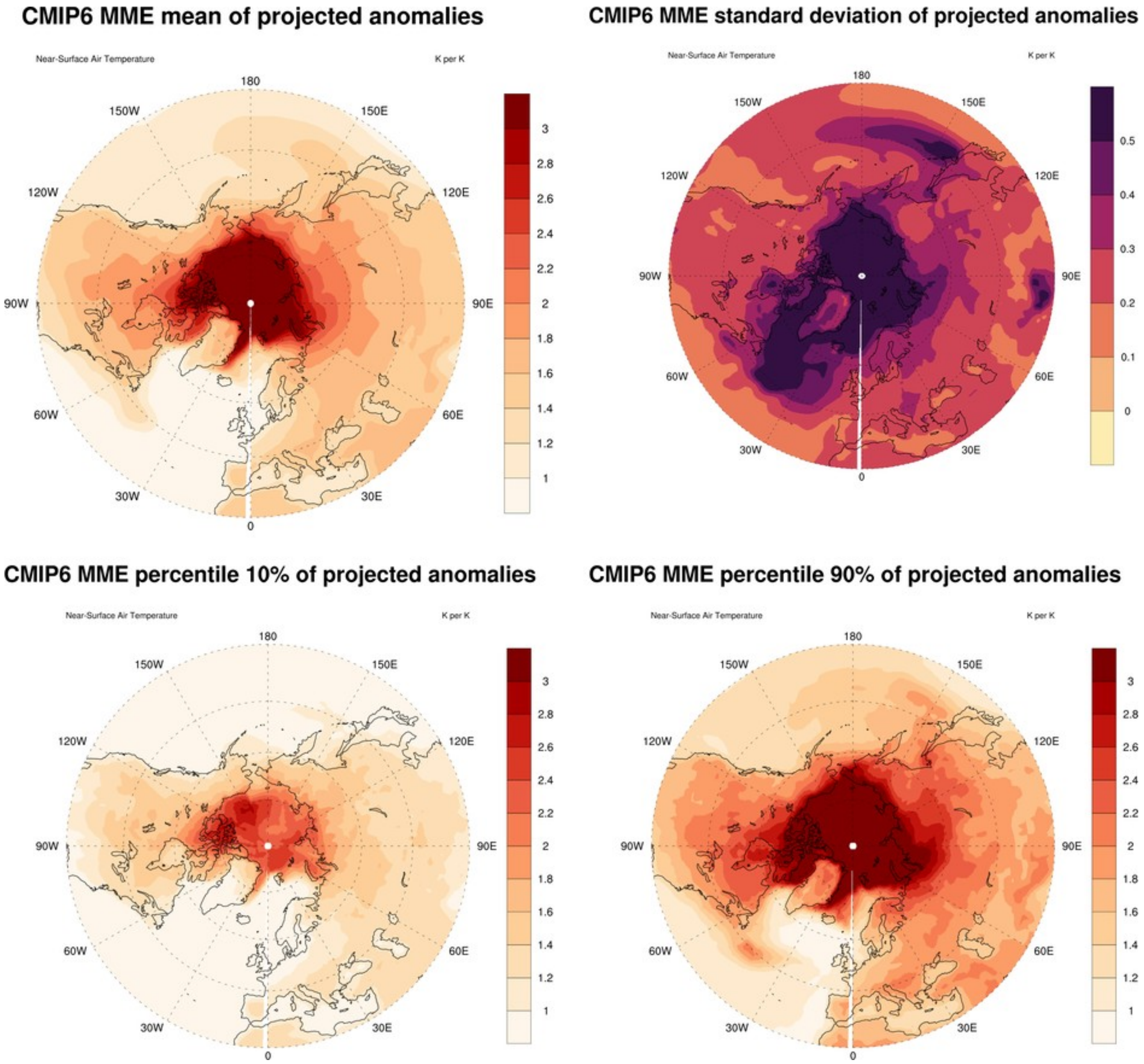

Fig. S2: Same as Fig. 1 but for mid-century (2041-2060) rather than late-century (2081-2100) anomalies (K per 1K of global warming).

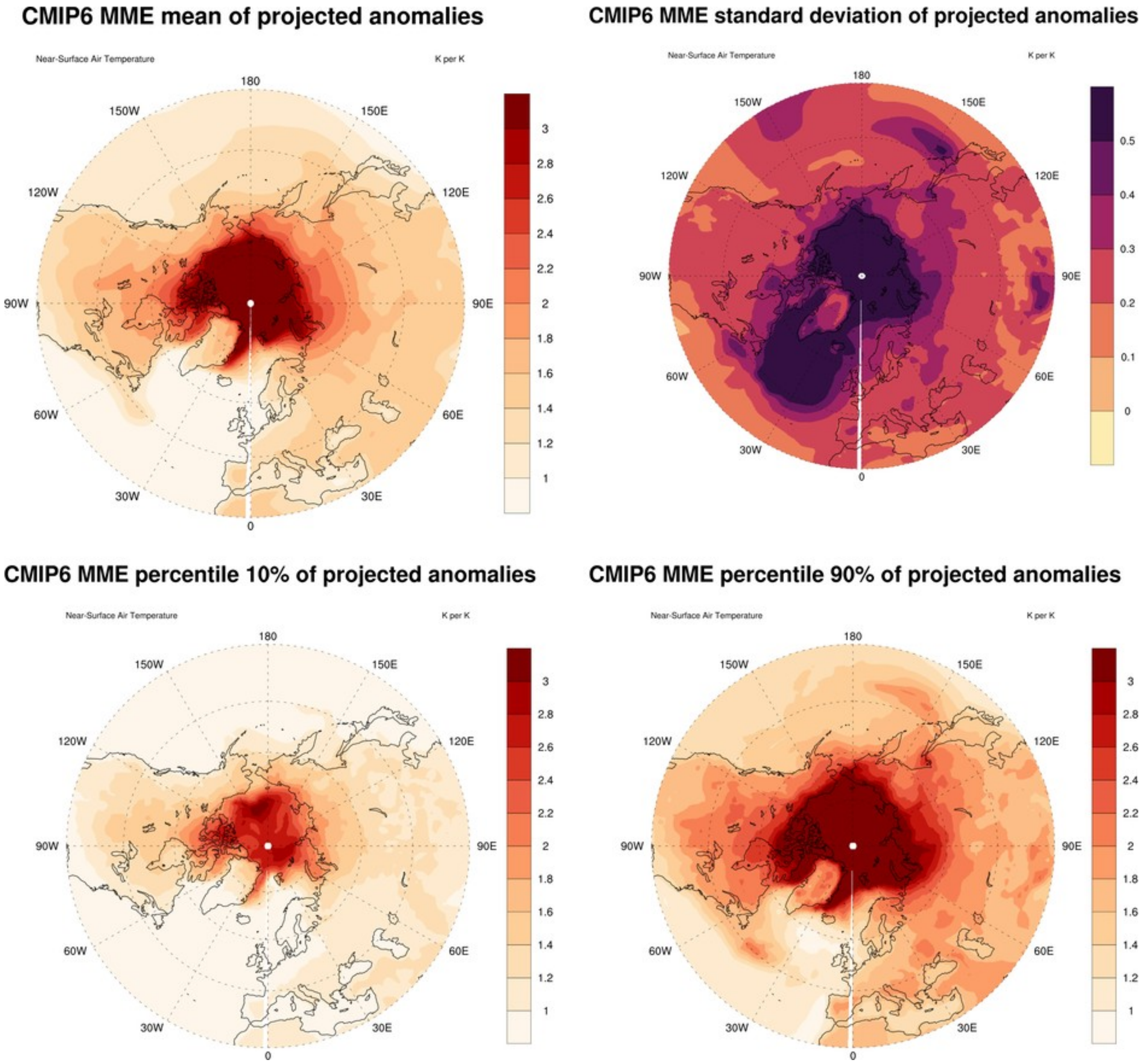

Fig. S3: Same as Fig. 1 but for the intermediate (SSP2-4.5) rather than high-emission (SSP5-8.5) CMIP6 scenario (K per 1K of global warming).

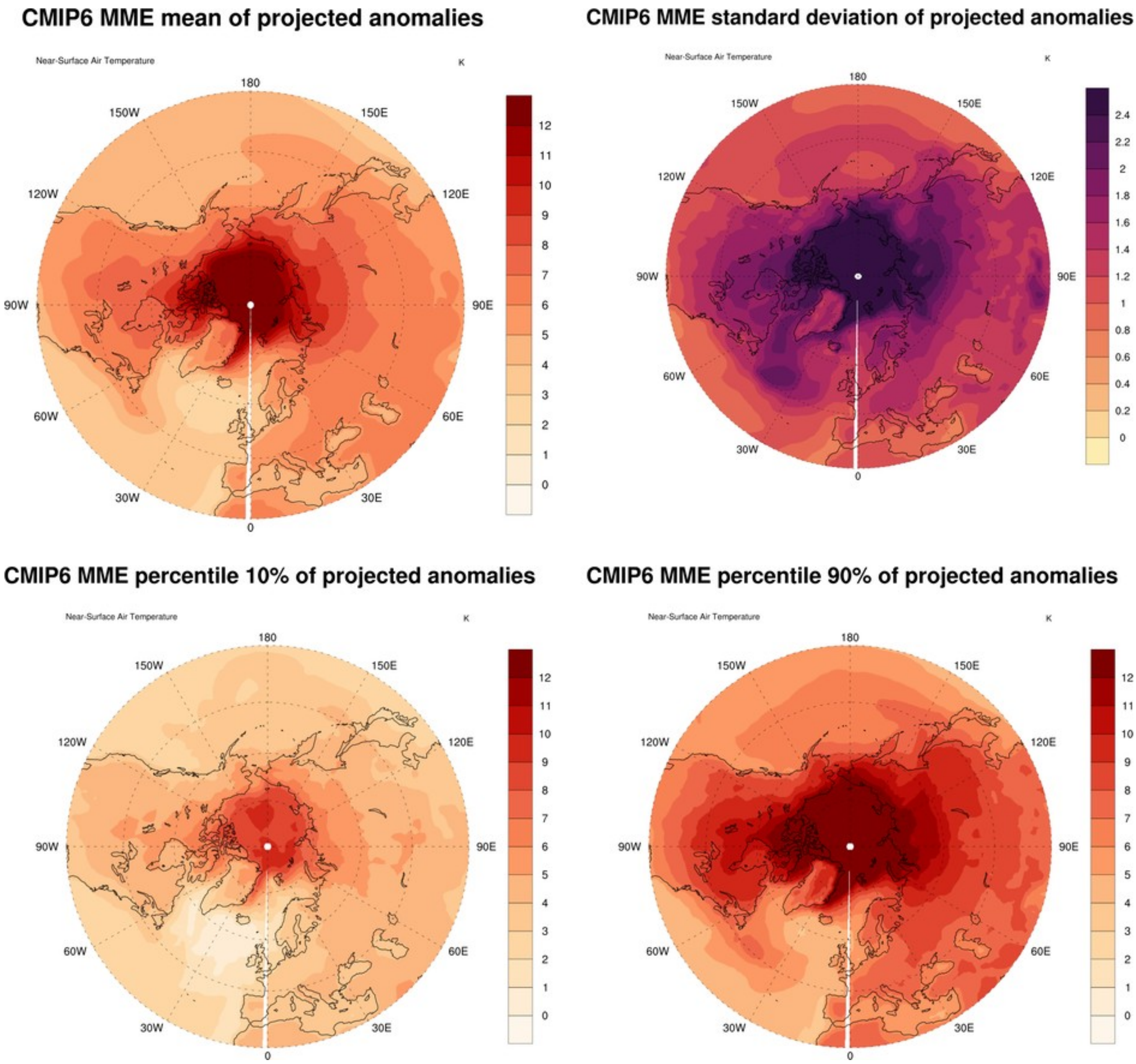

Fig. S4: Same Fig. 1 but without scaling by global warming (ONDJFM near-surface temperature anomalies in K estimated as the difference between 2081-2100 and 1995-2014 in the SSP5-8.5 high-emission scenario).

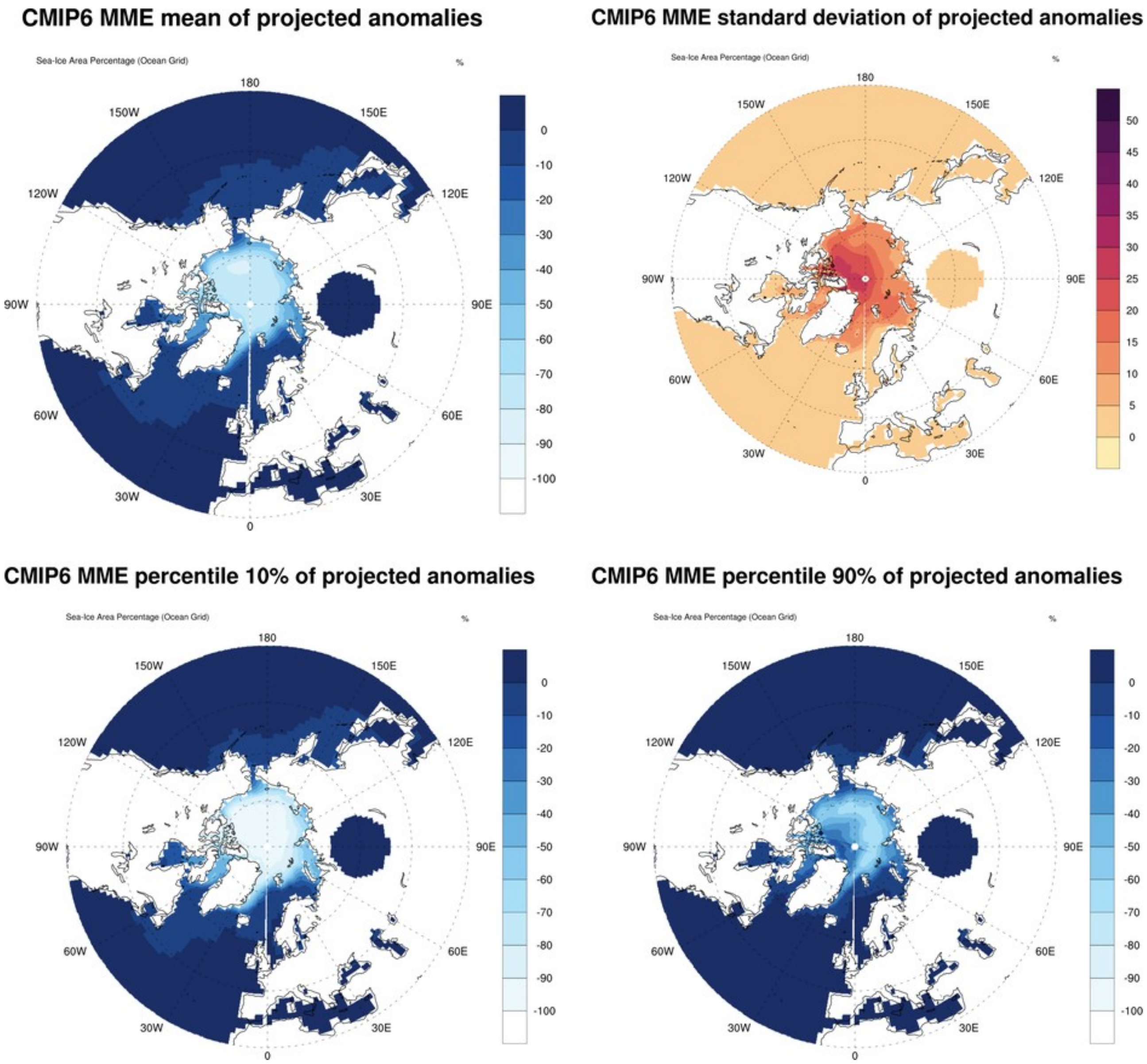

Fig. S5: As in Fig. S4 but for changes in sea ice concentration (%).

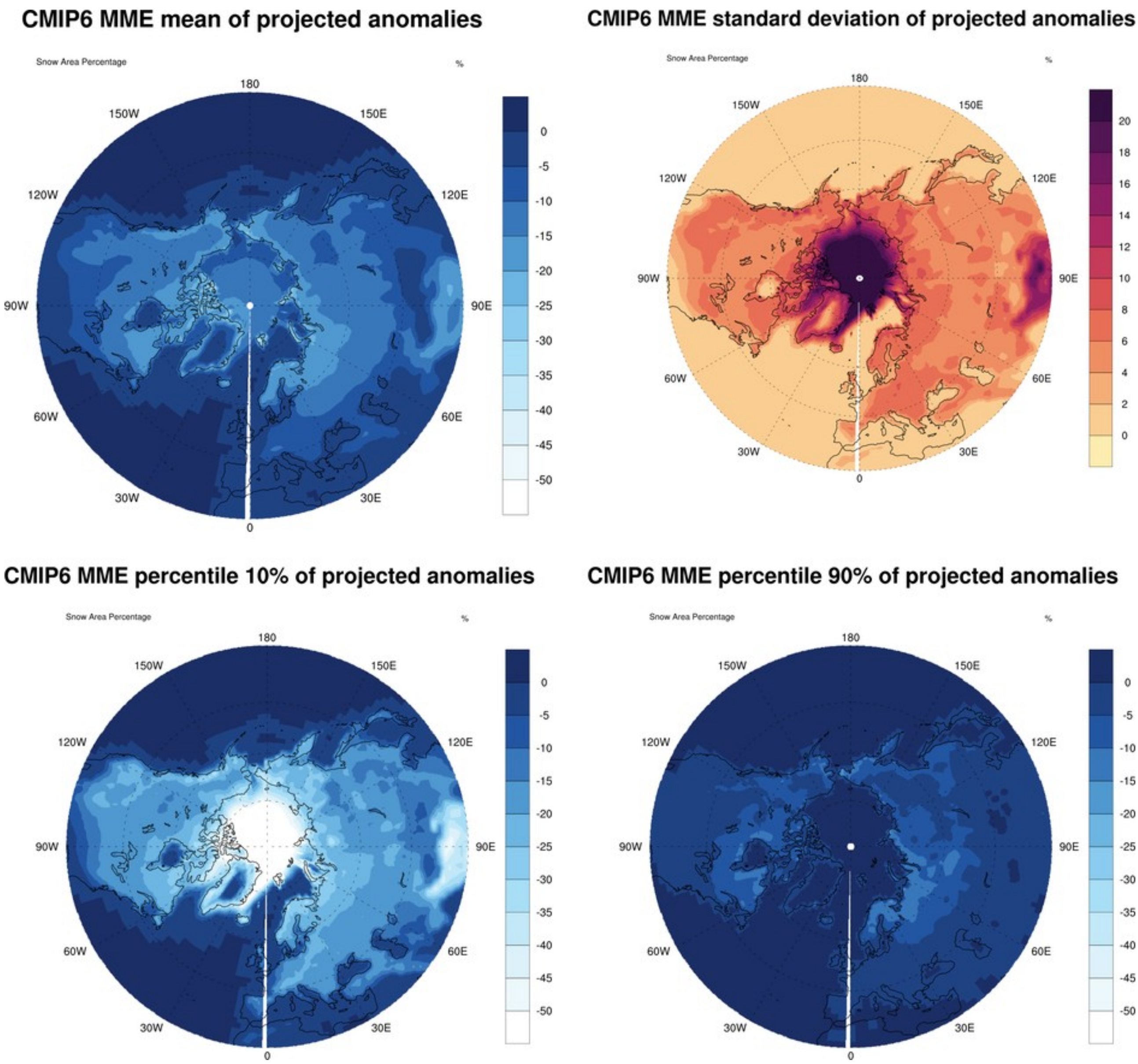

Fig. S6: As in Fig. S4 but for changes in snow cover (%). Note that the 90% local percentile (bottom right panel) of the projected snow anomalies over the Arctic indicates that some CMIP6 models still do not simulate the snow accumulation over sea ice.

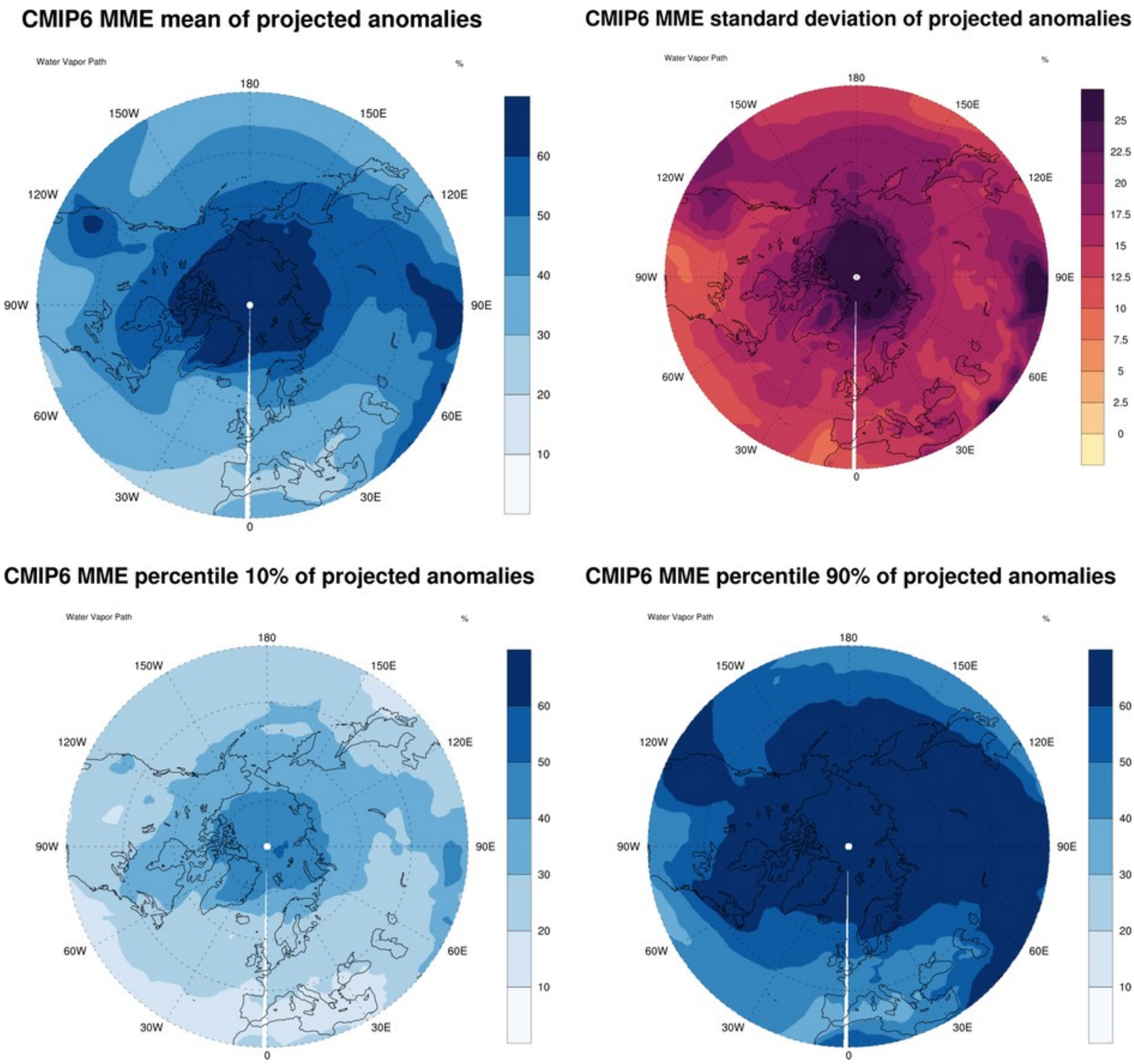

Fig. S7: As in Fig. S4 but for relative changes in total precipitable water (%).

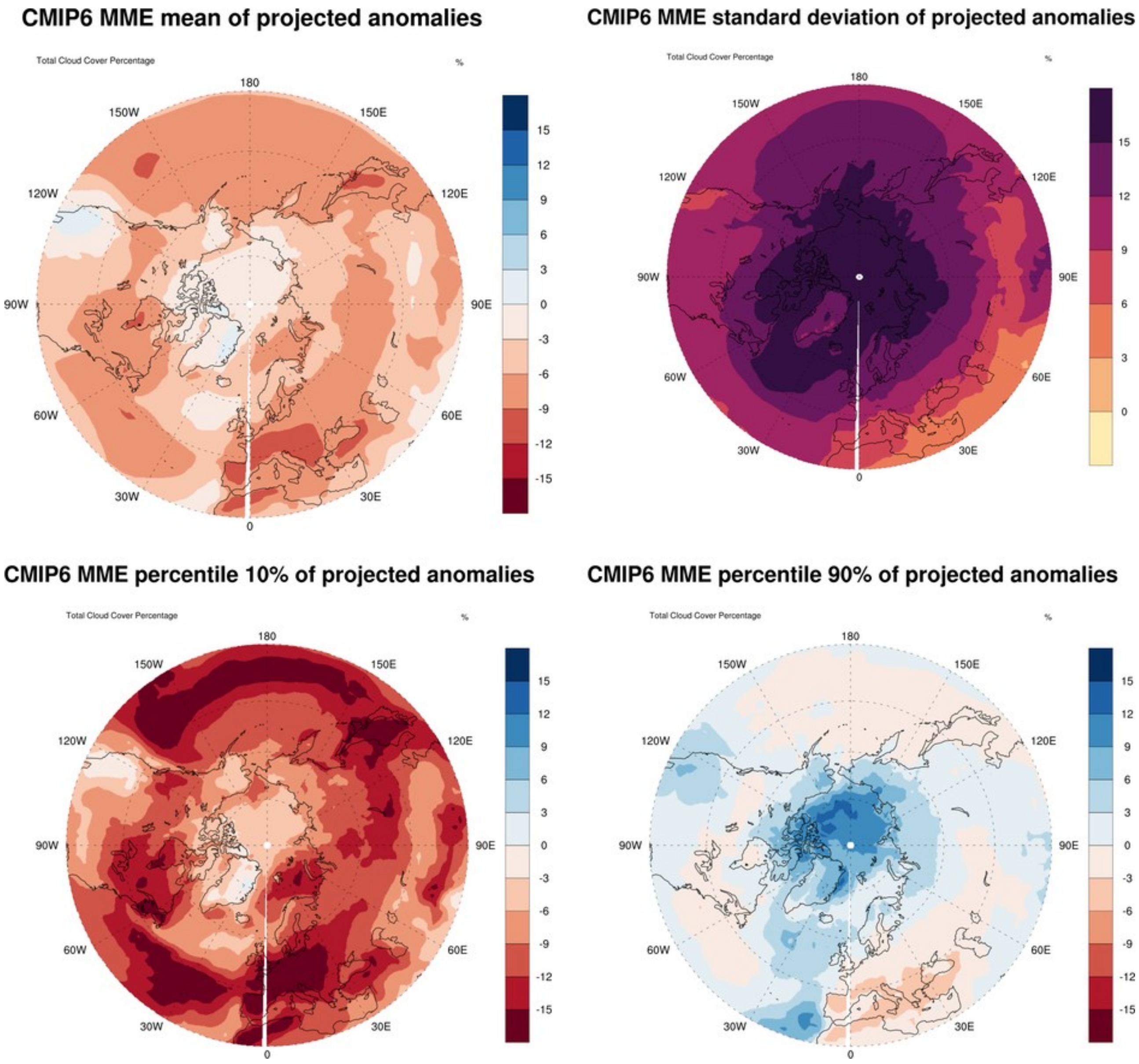

Fig. S8: As in Fig. S4 but for changes in total cloud cover (%).

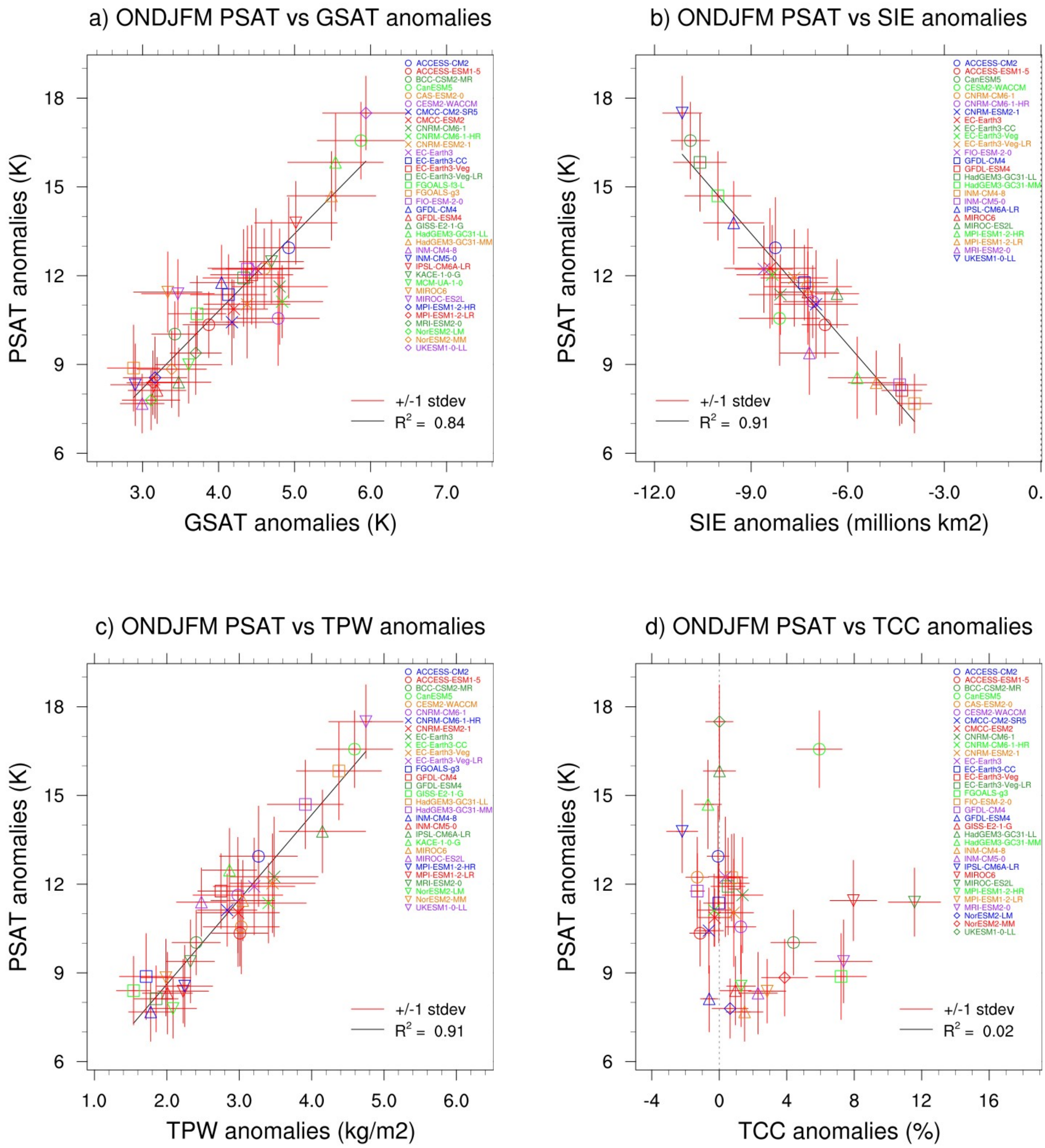

Fig. S9: Scatterplots of polar warming (i.e., ONDJFM PSAT anomalies) versus other metrics across CMIP6 models. a) Global warming (GSAT anomalies in K), b) ONDJFM sea ice extent anomalies (in millions of km²), c) Total Precipitable Water anomalies (in %), and d) Total Cloud Cover anomalies (in %). All anomalies are estimated over 2080-2099 versus the 1995-2014 baseline period. All models are not available for all metrics. Red error bars denote +/-1 standard deviation of interannual variability, while R² denotes the square coeeficient of the correlation between the two variables shown in each panel (Same as Fig. 2 but without substracting GSAT from PSAT anomalies).

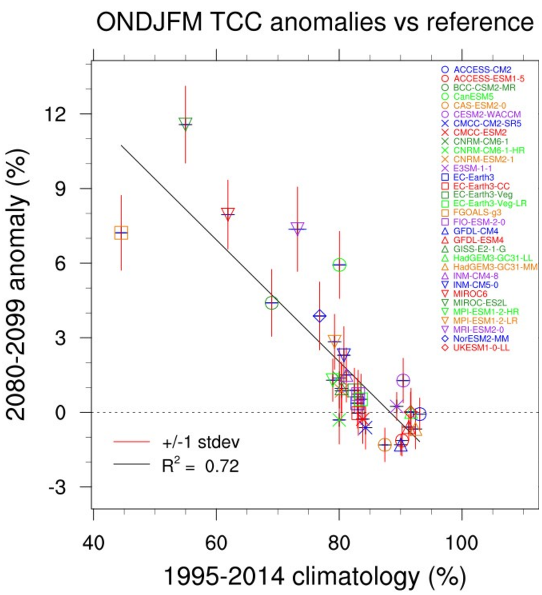

Fig. S10: Scatterplots of ONDJFM changes in Total Cloud Cover (%) versus present-day climatology (%) north of 60°N across CMIP6 models. Red vertical error bars denote +/-1 standard deviation of interannual variability in the anomalies. Similarly blue horizontal error bars characterize the present-day interannual variability but are very small given the low values found over the northern latitudes. The CMIP6 models that show the strongest increase at the end of the 21st century are clearly those that show the weakest (lower than observed) present-day values. Note for instance that the climatological average over the same domain, season and period is around 82% in ERA5.

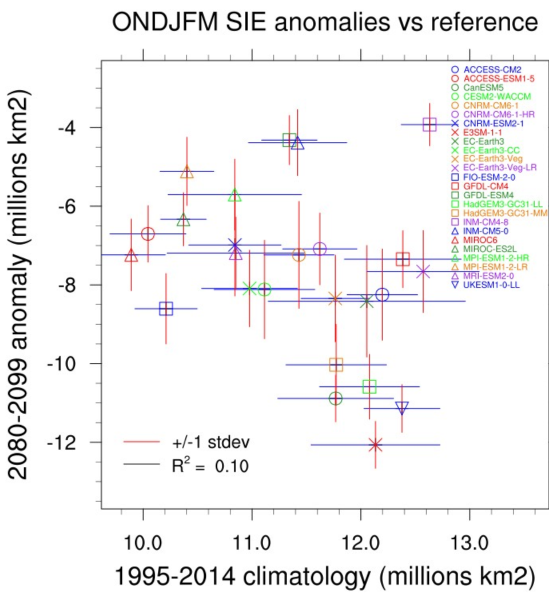

Fig. S11: Same as Fig. S10 but for ONDJFM sea ice extent (in millions of km²). Note that no relationship is found between mean state and future changes and that the present-day sea ice extent shows a large interannual variability (as indicated by the blue horizontal error bars).

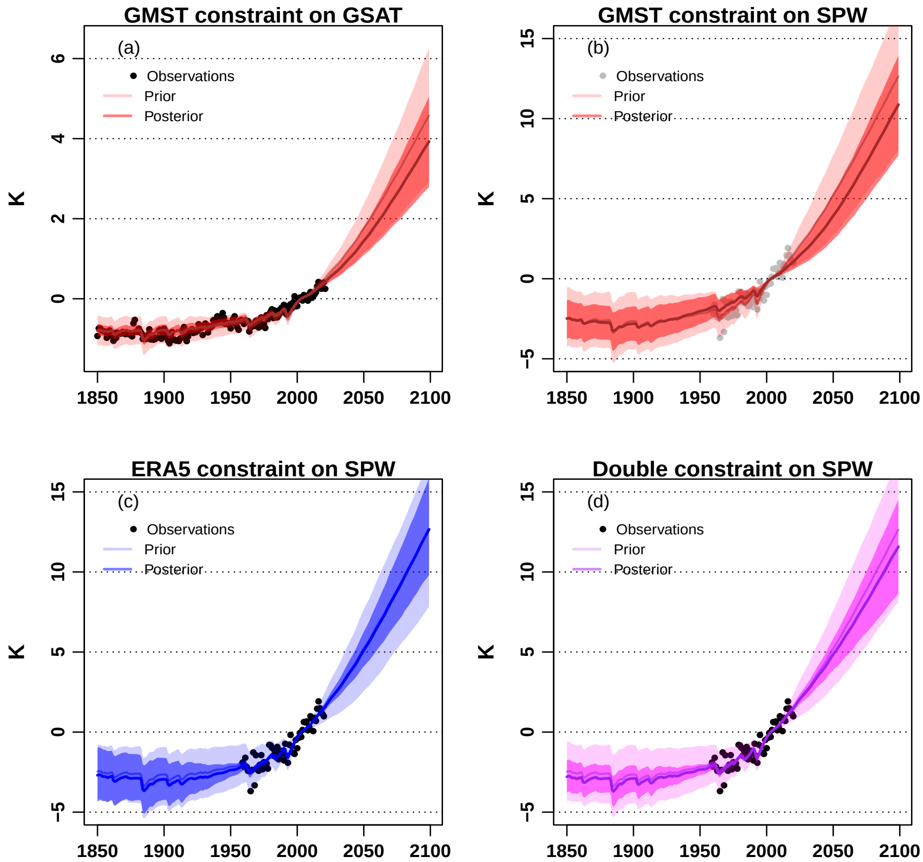

Fig. S12: Same as Fig. 4, but for the near-surface polar warming (SPW, north of 60°N) in K. KCC here leads to a narrowing of CMIP6 model uncertainty (5-95% confidence interval) by 31.3, 33.0 and 35.4% at the end of the 21st century in panels b (GMST only), c (ERA5 sea ice extent only) and d (both constraints) respectively. Note that the reduction of short-term and mid-term model uncertainties is much stronger than at the end of the century.

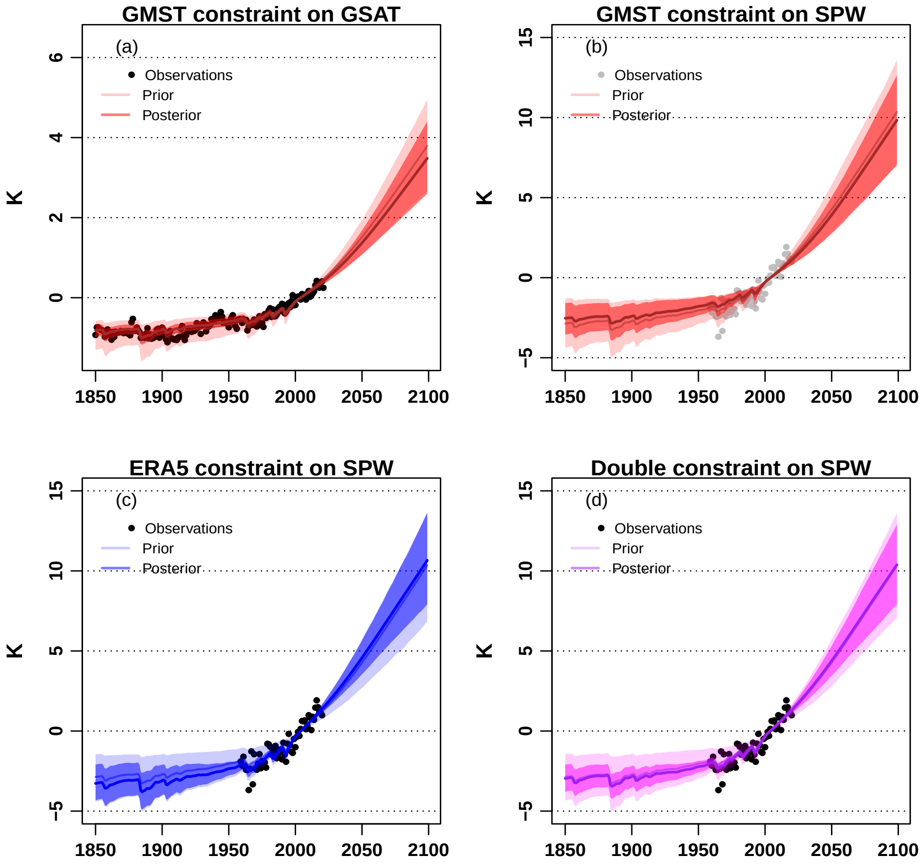

Fig. S13: Same as Fig. S12, but for the RCP8.5 high-emission scenario with 28 CMIP5 models.

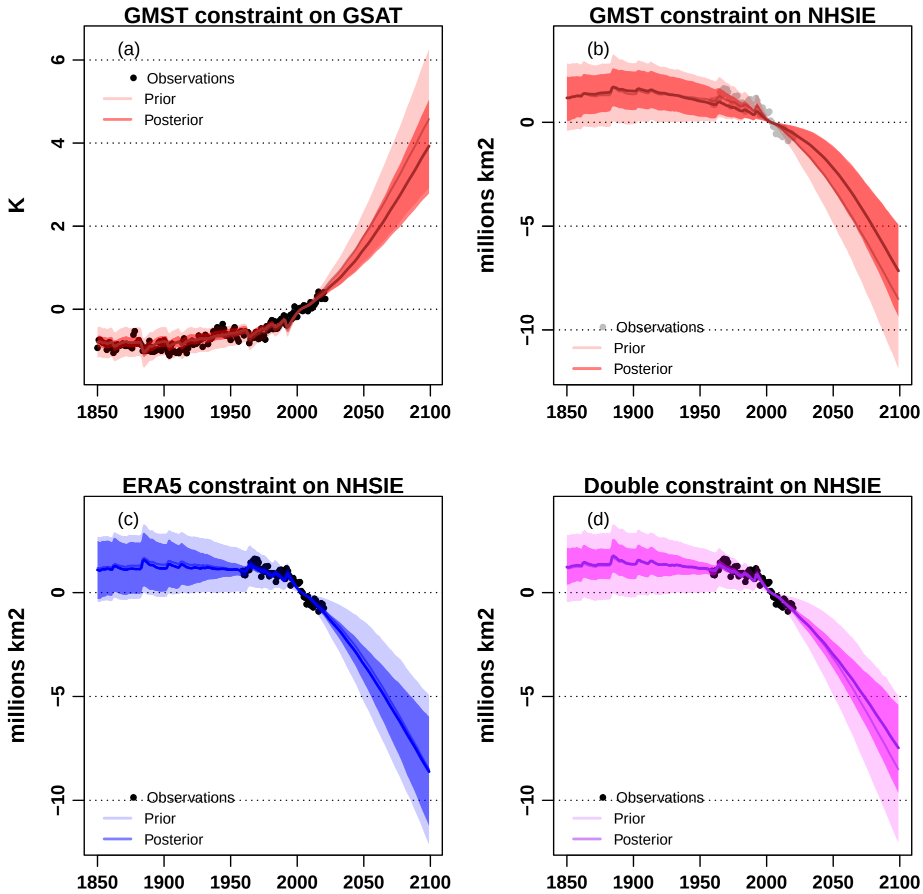

Fig. S14: Same as Fig. S12, but for the projected ONDJFM anomalies in northern hemisphere sea ice extent (NHSIE, in millions of km²). KCC here leads to a narrowing of CMIP6 model uncertainty (5-95% confidence interval in shading) by 35.5, 27.0 and 40.4% at the end of the 21st century in panels b (GMST only), c (ERA5 sea ice extent only) and d (both constraints) respectively. Note that the reduction of short-term and mid-term model uncertainties is much stronger than at the end of the century.

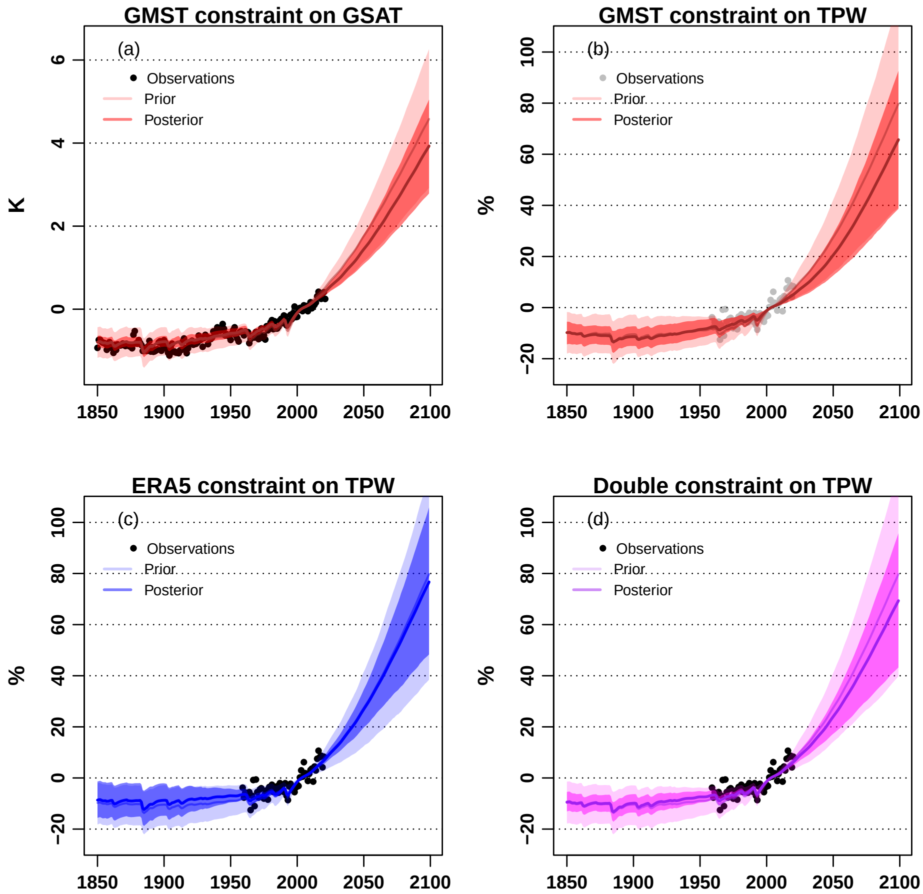

Fig. S15: Same as Fig. S12, but for the projected ONDJFM relative anomalies in total precipitable water (TPW, in %) averaged north of 60°N. KCC here leads to a narrowing of CMIP6 model uncertainty (5-95% confidence interval in shading) by 33.7, 28.4 and 34.4% at the end of the 21st century in panels b (GMST only), c (ERA5 sea ice extent only) and d (both constraints) respectively. Note that the reduction of short-term and mid-term model uncertainties is much stronger than at the end of the century. Not surprisingly, GMST is here the main observational constraint, in line with our former study[33] suggesting that global warming occurs at near-constant tropospheric relative humidity.

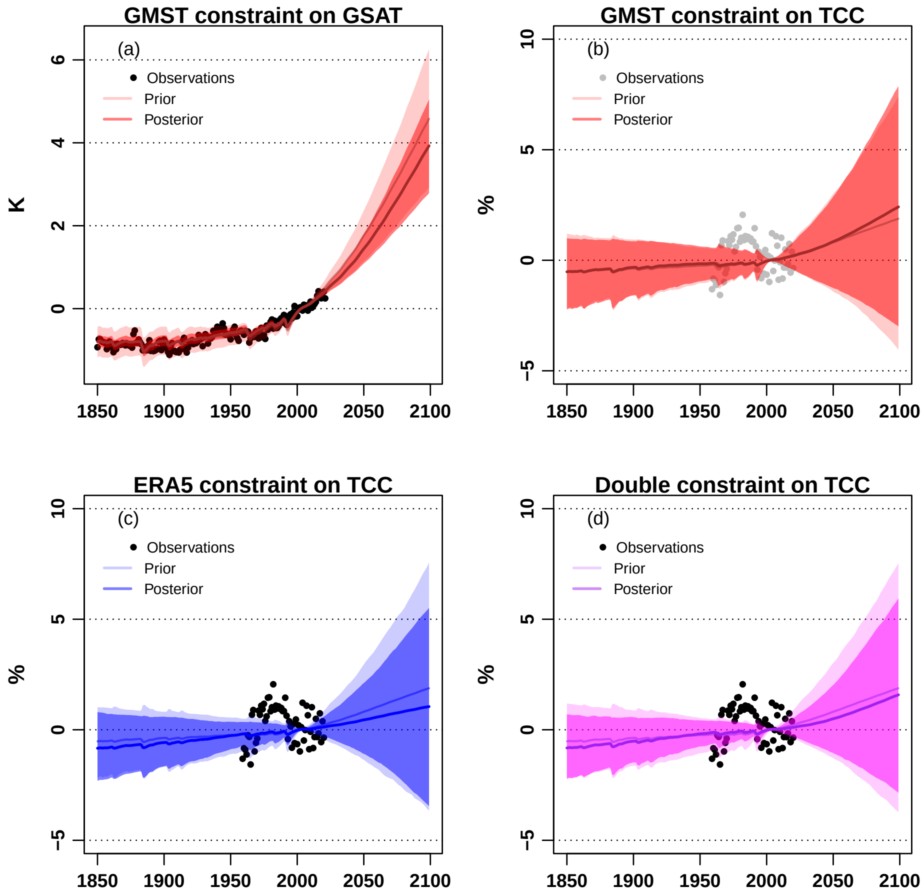

Fig. S16: Same as Fig. S12, but for the projected ONDJFM anomalies in total cloud cover (TCC, in %) averaged north of 60°N. KCC here leads to a limited narrowing of CMIP6 model uncertainty (5-95% confidence interval in shading). Moreover, the ERA5 multi-decadal variations may be partly due to a spurious effect of multiple changes in the observing system. Yet, global versus regional observational constraints still have complementary effects on the CMIP6 projections.

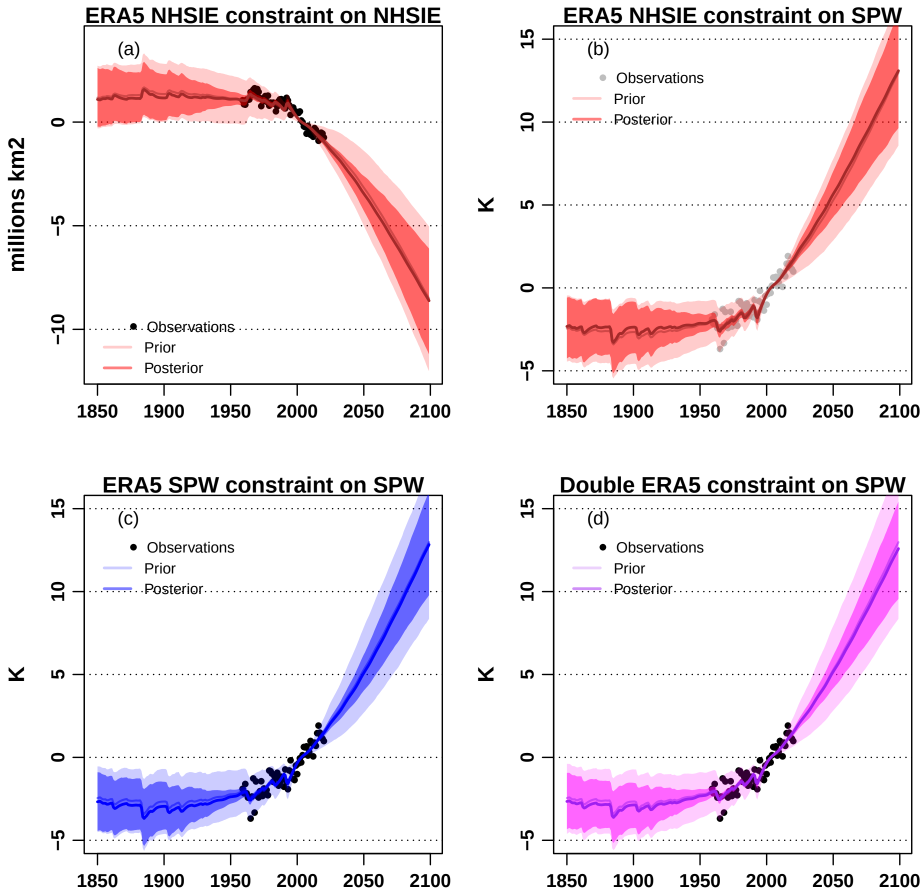

Fig. S17: Same as Fig. S12, but using only ERA5 to constrain projected ONDJFM polar near-surface air temperature (PSAT, in K) anomalies averaged north of 60°N. KCC here leads to a narrowing of CMIP6 model uncertainty (5-95% confidence interval in shafing) by 22.4, 31.0 and 36.6% at the end of the 21st century in panels b (ERA5 NHSIE only), c (ERA5 PSAT only) and d (both ERA5 constraints) respectively. Note that the number of CMIP6 models is slighly lower than in Fig. S12 due to the limited availability of sea ice concentration model outputs. Note also that the reduction of the 5-95% confidence interval is slighly lower than in Fig. 12, but stronger for the combined (i.e., doubled) constraint, thereby indicating less redundancy between the two observational constraints.

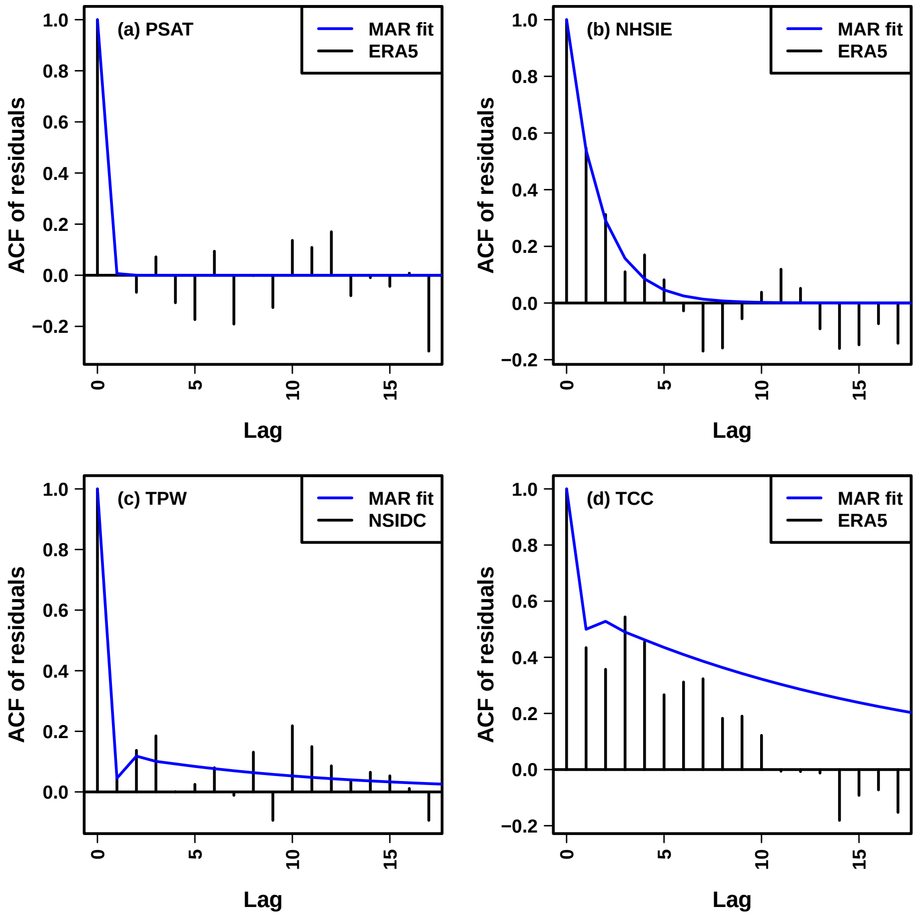

Fig. S18: Estimation of observed internal variability. Auto-correlation function of the "observed internal variability", i.e. ERA5 residuals of observed PSAT, NHSIE, northern high-latitude TPW, and northern high latitude TCC spatially-agregated ONDJFM indices after subtracting the raw CMIP6 multi-model mean forced response to the observed time-series. The autocorrelation of the MAR process fitted to the same residual time-series is shown in blue. The MAR process captures the slow decrease of auto-correlation typically at lags 1-5 for the Arctic sea ice extent (NHSIE). In contrast the slow decrease of the TCC auto-correlation is not well captured but may the artifact of a spurious multidecadal variability due to multiple changes in the observing system.